

Article

Chemically induced degradation of sirtuin 2 (Sirt2) by a proteolysis targeting chimera (PROTAC) based on sirtuin rearranging ligands (SirReals)

Matthias Schiedel, Daniel Herp, Sören Hammelmann, Sören Swyter, Attila Lehotzky, Dina Robaa, Judit Olah, Judit Ovádi, Wolfgang Sippl, and Manfred Jung

J. Med. Chem., **Just Accepted Manuscript** • DOI: 10.1021/acs.jmedchem.6b01872 • Publication Date (Web): 05 Apr 2017

Downloaded from <http://pubs.acs.org> on April 6, 2017

Just Accepted

“Just Accepted” manuscripts have been peer-reviewed and accepted for publication. They are posted online prior to technical editing, formatting for publication and author proofing. The American Chemical Society provides “Just Accepted” as a free service to the research community to expedite the dissemination of scientific material as soon as possible after acceptance. “Just Accepted” manuscripts appear in full in PDF format accompanied by an HTML abstract. “Just Accepted” manuscripts have been fully peer reviewed, but should not be considered the official version of record. They are accessible to all readers and citable by the Digital Object Identifier (DOI®). “Just Accepted” is an optional service offered to authors. Therefore, the “Just Accepted” Web site may not include all articles that will be published in the journal. After a manuscript is technically edited and formatted, it will be removed from the “Just Accepted” Web site and published as an ASAP article. Note that technical editing may introduce minor changes to the manuscript text and/or graphics which could affect content, and all legal disclaimers and ethical guidelines that apply to the journal pertain. ACS cannot be held responsible for errors or consequences arising from the use of information contained in these “Just Accepted” manuscripts.

1
2
3
4
5
6
7 Chemically induced degradation of sirtuin 2 (Sirt2)
8
9
10
11 by a proteolysis targeting chimera (PROTAC) based
12
13
14
15 on sirtuin rearranging ligands (SirReals)
16
17
18
19
20

21 *Matthias Schiedel,^{†∇} Daniel Herp,[†] Sören Hammelmann,[†] Sören Swyter,[†] Attila Lehotzky,[§] Dina*
22 *Robaa[◇], Judit Oláh,[§] Judit Ovádi,[§] Wolfgang Sippl,[◇] Manfred Jung^{†||*}*
23
24
25

26
27 [†] Institute of Pharmaceutical Sciences, University of Freiburg, Albertstraße 25, 79104 Freiburg
28 im Breisgau, Germany
29
30
31

32 [§] Institute of Enzymology, Research Centre for Natural Sciences, Hungarian Academy of
33 Sciences, Magyar Tudósok körútja 2, H 1117 Budapest, Hungary
34
35
36

37
38 [◇] Institute of Pharmacy, Martin-Luther-University Halle-Wittenberg, Wolfgang-Langenbeck-
39 Straße 4, 06120 Halle (Saale), Germany
40
41
42

43
44 ^{||} Freiburg Institute of Advanced Studies (FRIAS), University of Freiburg, Albertstraße 19,
45 79104 Freiburg im Breisgau, Germany
46
47
48

49
50
51
52
53
54 KEYWORDS: epigenetics, histone deacetylases, sirtuins, protein degradation, PROTAC
55
56
57
58
59
60

1
2
3 ABSTRACT: Here we report the development of a proteolysis targeting chimera (PROTAC)
4 based on the combination of the unique features of the sirtuin rearranging ligands (SirReals) as
5 highly potent and isotype-selective Sirt2 inhibitors with thalidomide, a bona fide cereblon ligand.
6
7
8 For the first time, we report the formation of a PROTAC by Cu(I)-catalyzed cycloaddition of a
9 thalidomide-derived azide to an alkynylated inhibitor. This thalidomide-derived azide as well as
10 the highly versatile linking strategy can be readily adapted to alkynylated ligands of other
11 targets. In HeLa cells, our SirReal-based PROTAC induced isotype-selective Sirt2 degradation
12 that results in the hyperacetylation of the microtubule network coupled with enhanced process
13 elongation. Thus, our SirReal-based PROTAC is the first example of a probe that is able to
14 chemically induce the degradation of an epigenetic eraser protein.
15
16
17
18
19
20
21
22
23
24
25
26
27
28
29
30
31

32 INTRODUCTION

33
34
35 Until today, 18 different lysine deacetylases (KDACs) have been identified in the human
36 genome and grouped into four classes, according to their sequence homology to yeast KDACs.¹
37 These enzymes are able to remove acyl groups from the ϵ -amino group of acylated lysine
38 residues. Sirtuins, which had been initially described as class III histone deacetylases (HDACs)
39 or Sir2 proteins,² form a very special class of the KDAC family. Sirtuins use NAD^+ as a cofactor
40 and constitute the class III KDACs, while the deacetylases of classes I, II, and IV are prime
41 examples of Zn^{2+} -dependent metalloproteases. The human genome encodes seven isotypes of
42 sirtuins (Sirt1-7), which differ in their catalytic activity as well as in their subcellular
43 localization.³ Moreover, sirtuins show no sequence homology to the Zn^{2+} -dependent KDACs.
44
45
46
47
48
49
50
51
52
53
54
55
56
57
58
59
60

1
2
3 deacetylation. Sirtuins are also able to cut off other acyl groups, such as crotonyl,⁴ glutaryl,⁵
4 succinyl,⁶ myristoyl,⁷ and palmitoyl⁸ from the ϵ -amino group of acylated lysines. The
5
6 deacetylase activity of Sirt6 and Sirt7 was recently shown to be upregulated by long-chain fatty
7
8 acids and nucleic acids, respectively.^{7, 9} Besides histones, a variety of non-histone proteins have
9
10 been reported as sirtuin substrates in recent years, e.g. α -tubulin,¹⁰ p53,¹¹ BubR1,¹² and NF κ B.¹³
11
12 By regulating the acylation state of their protein substrates, sirtuins have been implicated in
13
14 influencing a multitude of cellular processes such as transcription,¹⁴ metabolic sensing,¹⁵
15
16 inflammation,¹⁶ aging,¹⁷ and apoptosis.¹⁵ The isotype Sirt2, which is predominantly localized in
17
18 the cytoplasm, was shown to have a major impact on cell cycle regulation,¹⁰ autophagy,¹⁸
19
20 peripheral myelination,¹⁹ and immune and inflammatory response.²⁰ Furthermore, a number of
21
22 reports implicate that the overall cellular agenda of Sirt2 is not only dependent on its catalytical
23
24 activity but also on its protein-protein interactions with binding partners, e.g. KDAC6,¹⁰
25
26 HOXA10,²¹ and 14-3-3 β/γ .²² A dysregulation of Sirt2 has been associated with the pathogenesis
27
28 of bacterial infections,^{20b, 20c} type II diabetes,²³ neurodegenerative diseases,²⁴ and cancer,²⁵ which
29
30 makes Sirt2 a promising target for pharmaceutical intervention. However, for some disease
31
32 scenarios, e.g. Huntington's disease, it is not perfectly clear if Sirt2 has to be up- or
33
34 downregulated respectively inhibited to ameliorate specific disease conditions.²⁶ Many cell-
35
36 based or animal studies have tried to address these unanswered questions. Yet, they have been
37
38 hampered by the lack of suitable tool compounds, which show sufficient isotype selectivity as
39
40 well as pharmacokinetic properties. The urgent need for such tool compounds, to further
41
42 investigate the cellular effects of Sirt2-dependent deacetylation as well as their consequences on
43
44 downstream signaling, led to the discovery of a number of Sirt2-selective small molecule
45
46 inhibitors.²⁷ However, Sirt2-selective and drug-like inhibitors with an identified binding mode,
47
48
49
50
51
52
53
54
55
56
57
58
59
60

that enables the structure-based discovery of molecular tools for Sirt2, are still extremely scarce.

Recently, we discovered a new class of Sirt2-selective and highly potent inhibitors (Fig. 1).²⁸

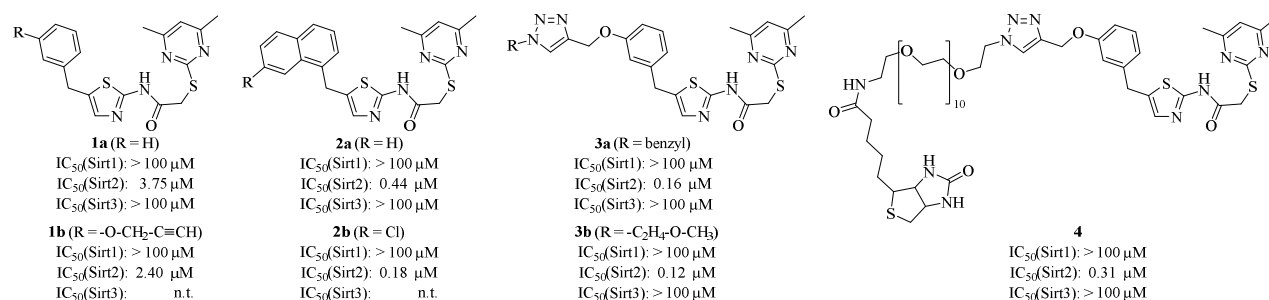


Figure 1. Chemical structures and inhibition data of selected SirReals (**1a/b-3a/b**) and the SirReal-based affinity probe for Sirt2 (**4**).

The co-crystal structures of Sirt2 in complex with **1a** or **2a**, which were the first crystal structures of Sirt2 complexed with Sirt2-selective small-molecule inhibitors, revealed a unique mode of inhibition that is characterized by a major rearrangement of Sirt2's active site upon ligand binding. Therefore, these inhibitors were referred to as sirtuin rearranging ligands (SirReals).²⁸ By structure-guided optimization and extensive structure-activity relationship (SAR) studies we were able to discover the SirReal analogues **2b** and **3a/b** with enhanced potency and cellular efficacy.²⁹ The triazole-based SirReals **3a/b**, which additionally show improved water solubility, were initially prepared to validate the design of our Sirt2 affinity probe (**4**). The co-crystal structure of Sirt2 complexed with **3a**, revealed an extended binding mode of the triazole-based SirReals compared to their parent compound **1a** (Fig 2).

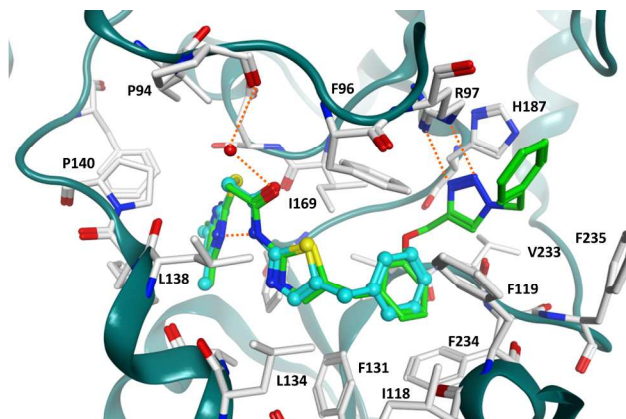


Figure 2. Comparison of the binding mode of SirReal1 **1a** (from PDB ID 4RMI, colored cyan) and the triazole-based SirReal **3a** (from PDB ID 5DY5, colored green) at Sirt2 (PDB ID 5DY5). Hydrogen bonds are shown as dashed orange lines, the conserved water molecule bridging the interaction of the SirReals is shown as red ball.

The triazole moiety further extends into the acyllysine binding channel where it forms a hydrogen bond with Arg 97. This results in a more efficient blockade of the substrate binding site. Since the *N*-substituent at the triazole moiety protrudes towards the entry of the acyllysine channel (see Fig. 2), we proceeded to attach larger residues to the triazole moiety aiming to expose certain functional labels to the protein surface. This approach was successfully validated by the development of the biotinylated SirReal-based affinity probe for Sirt2 (**4**), which was shown to be suitable for pull-down experiments as well as biolayer interferometry.^{29b} To probe the cellular effects of Sirt2, not only by occupancy-based small molecule inhibition of its deacylase activity but also by eliminating the protein with all its scaffolding functions from the cellular network, we were highly interested in applying our protocol for the development of Sirt2-selective probes to the concept of chemically induced protein degradation. This concept is based on bifunctional small molecules, so called proteolysis targeting chimeras (PROTACs). These molecular tools are capable to hijacking the cellular quality control by recruiting the

1
2
3 protein of interest (POI) to E3 ubiquitin ligases for polyubiquitinylation and thus to induce its
4
5 proteasomal degradation.³⁰ Since its first description by Crews and co-workers in the year 2001,
6
7 the PROTAC concept has been widely applied to induce the degradation of various proteins,
8
9 such as kinases,³¹ transcription factors,³² and epigenetic reader proteins.³³ However, neither
10
11 epigenetic writer nor epigenetic eraser proteins have been addressed by PROTACs, yet. In terms
12
13 of a potential therapeutic application the PROTAC strategy offers several advantages compared
14
15 to occupancy-based enzyme inhibition. For example, there is no need to maintain high in vivo
16
17 concentrations to ensure sufficient enzyme inhibition, which reduces the risk of off-target side
18
19 effects.³⁰ In this study, we report the development of a PROTAC based on the combination of the
20
21 unique features of the sirtuin rearranging ligands (SirReals) as highly potent and isotype-
22
23 selective Sirt2 inhibitors with thalidomide, a bona fide ligand for the E3 ubiquitin ligase
24
25 cereblon. So far, thalidomide has been attached by amide coupling procedures to the target
26
27 ligand of interest.³⁴ Here, we report for the first time a protocol for the development of a triazole-
28
29 derived PROTAC, which is based on a Cu(I)-catalyzed cycloaddition of an azido-thalidomide-
30
31 conjugate to an alkynylated ligand for the targeted protein, in this case Sirt2. Molecular
32
33 modelling of the ternary complex of Sirt2, cereblon and the chimera proposes a binding model of
34
35 the interaction of the bifunctional ligand is with both binding pockets.
36
37
38
39
40
41
42
43

44 RESULTS

45
46
47 For the design of the SirReal-based PROTAC we combined the structural features of the
48
49 Sirt2-selective and highly potent triazole-based SirReals (see Fig.1) with the cereblon ligand
50
51 thalidomide. We have based the design of our PROTAC on the cereblon recruiting thalidomide,
52
53 since this approach has already been used to efficiently induce the depletion of epigenetically
54
55 active proteins, e.g. the Bromo- and Extra-Terminal domain (BET) family.^{33a, 33b} Furthermore,
56
57
58
59
60

1
2
3 thalidomide was chosen over other E3 ubiquitin ligase recruiting moieties such as nutlin³⁵ or
4
5 VHL ligands^{33c} due to its straightforward synthetic accessibility. Based on our previous work on
6
7 a SirReal-based affinity probe^{29b} as well as the study of Winter et al.,^{33b} we already had valid
8
9 information on where to place the linker without losing affinity to Sirt2 and cereblon,
10
11 respectively. From analysis of a generated model of Sirt2 complexed with cereblon (for details
12
13 see Methods section), we predicted a *N*-butyl-2-oxyacetamide linker to be suitable to recruit
14
15 Sirt2 to cereblon with an adequate proximity that allows an efficient ubiquitin transfer (Fig. 3).
16
17 The Sirt2-cereblon complex generated using program HADDOCK³⁶ was used to dock our
18
19 PROTAC (**12**). The docking results show that the SirReal and the thalidomide part of **12** is
20
21 interacting in a similar way as the original molecules in Sirt2 (PDB ID 5DY5)^{29b} and cereblon
22
23 (PDB ID 4CI2)³⁷ (Fig. 3B and Supporting Information, Fig. S2).
24
25
26
27
28
29
30
31
32

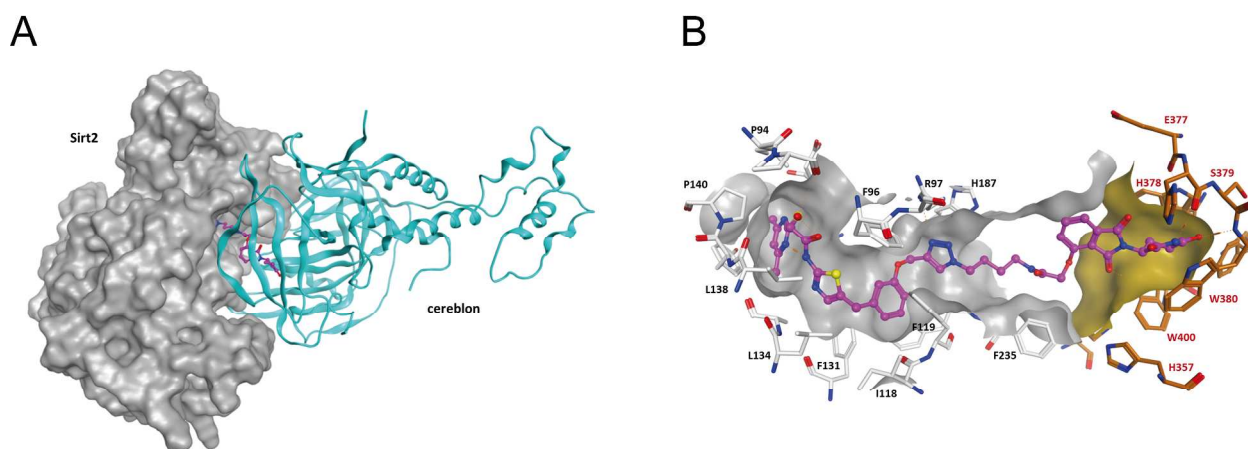
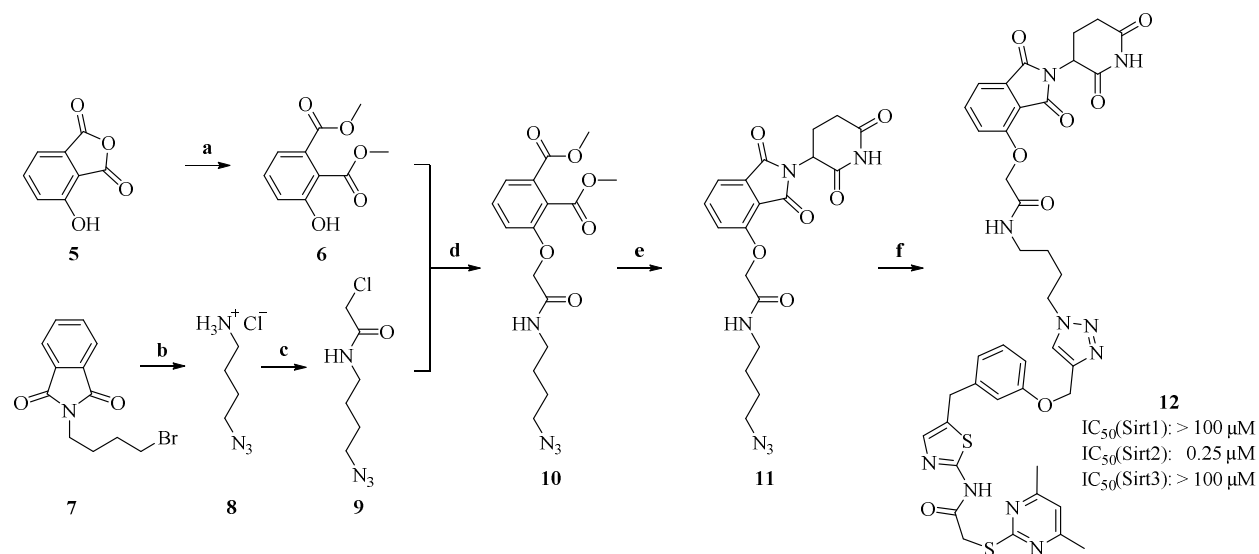


Figure 3. (A) Docking pose of the ternary Sirt2-**12**-cereblon complex. The surface of Sirt2 is displayed in white whereas cereblon is displayed as ribbon model. The PROTAC **12** is colored magenta. (B) Predicted binding mode for **12** (magenta) at the Sirt2-cereblon complex. The surface of the Sirt2 SirReal binding pocket is colored white, whereas the thalidomide binding pocket of cereblon is colored orange. Hydrogen bonds are shown as dashed orange lines.

1
2
3
4
5
6
7 To realize the envisaged SirReal-based PROTAC (**12**), we set up a convergent synthesis route
8 depicted in Scheme 1. While planning this synthesis route we focused our efforts on i) generating
9 the SirReal-based PROTAC **12**, capable of inducing Sirt2 degradation ii) providing a “click-
10 able” azido-thalidomide-conjugate as a versatile cereblon ligand ready for conjugation with other
11 alkynylated ligands. The first step of our synthesis route was the methanolysis of
12 3-hydroxyphthalic acid anhydride (**5**) to generate the dimethylester (**6**).³⁸ The 4-azidobutan-1-
13 aminium chloride (**8**) was prepared by a nucleophilic substitution of
14 *N*-(4-bromobutyl)phthalimide (**7**) with NaN₃ followed by hydrazinolysis.³⁹ Then, **8** was
15 chloroacetylated to obtain compound **9**. *O*-Alkylation of **6** by the alkyl chloride **9** gave
16 compound **10**. To synthesize the azido-thalidomide-conjugate (**11**), the dimethylester **10** was first
17 hydrolyzed to the dicarboxylic acid and then converted into the imide **11**, after activation with
18 *N,N'*-dicyclohexylcarbodiimide. Finally, compound **11** was conjugated with the propargylated
19 SirReal analogue **1b** through a Cu(I)-catalyzed Huisgen cycloaddition⁴⁰ to yield the SirReal-
20 based PROTAC (**12**).
21
22
23
24
25
26
27
28
29
30
31
32
33
34
35
36
37
38
39
40
41
42
43
44
45
46
47
48
49
50
51
52
53
54
55
56
57
58
59
60

Scheme 1. Synthesis and IC₅₀ values of SirReal-based PROTAC (**12**)^a

^aReagents and conditions: (a) methanol, thionyl chloride, 0 °C - 80 °C, 4 h, 63% yield; (b) NaN₃, DMF, rt, 12 h, then hydrazine monohydrate, ethanol, 0 °C - rt, 24 h, 99% yield; (c) chloroacetyl chloride, trimethylamine, DMF, 0 °C - rt, 1h, 82% yield; (d) Cs₂CO₃, acetonitrile, reflux, 5h, then rt, 12 h, 88% yield; (e) NaOH, ethanol, rt, 1.5 h, then 3-aminopiperidine-2,6-dione hydrochloride, *N,N*-dimethylpyridin-4-amine, trimethylamine, dichloromethane, *N,N'*-dicyclohexylcarbodiimide, 0 °C - rt, 22 h, 50% yield; (f) **1b**, sodium ascorbate, CuSO₄, water/*tert*-BuOH (1:1), 60 °C, 1 h, then rt, 16 h, 33% yield.

The SirReal-based PROTAC (**12**) was evaluated for its *in vitro* inhibition of Sirt1-3 in a fluorescence-based deacetylase activity assay as previously described.⁴¹ We detected a highly potent inhibition of Sirt2 with an IC₅₀ value of 0.25 μM ± 0.02 μM and as desired the deacetylase activity of isotypes Sirt1 and Sirt3 was only affected at concentrations higher than 100 μM (Scheme 1). To prove the suitability of our SirReal-based PROTAC (**12**) for chemically induced Sirt2 degradation, we assessed the cellular levels of Sirt2 in HeLa cells after incubation with **12** via Western blot analyses (Fig 4). To show the isotype selectivity of our probe, we determined the change in cellular levels of Sirt1 as well. As an experiment, to show that the Sirt2 degradation is not induced by the unlabeled ligand alone, we incubated the cells just with **3b**.

1
2
3 Indeed, **12** is capable of inducing isotype-selective degradation of Sirt2 (Fig. 4A). Moreover, we
4
5 were able to show that the effect of **12** on Sirt2 degradation can be counteracted either by
6
7 competition with the unlabeled ligand **3b** or by the proteasome inhibitor MG132 (Fig. 4B). The
8
9 dependence of Sirt2 depletion on the concentration of **12** is illustrated in Figure 4C. In the range
10
11 of 0.05 μ M to 5 μ M we were able to show a concentration-dependent effect of **12**. At higher
12
13 concentrations the efficacy of **12** is limited, which might be due to saturation effects on one of
14
15 the targets. No effects could be observed in the control experiments with **3b** and thalidomide,
16
17 neither in single treatment nor in combination (Fig. 4C). A more detailed time course of the
18
19 chemically induced Sirt2 degradation in HeLa cells due to treatment with **12** is given in Fig. 4D.
20
21 A maximum effect could be detected after 2 hours of treatment. In addition, the effect of **12** on
22
23 the level and distribution of Sirt2 was visualized in living HeLa cells expressing EGPF-Sirt2 by
24
25 fluorescence microscopy. Consistent with Western blot results, these studies indicate that
26
27 treatment with **12** results in reduced Sirt2 levels as well. Moreover, the dot-like pattern of the
28
29 fluorescence signal suggests enrichment of Sirt2 in proteasomes (Fig. 5).⁴² To investigate the
30
31 phenotype variation between cells treated with the Sirt2 enzymatic inhibitor **3b** and cells treated
32
33 with our PROTAC (**12**), we probed the acetylation levels of tubulin, a well-known Sirt2
34
35 substrate,¹⁰ via immunofluorescence microscopy. Depletion of Sirt2 due to treatment with **12**
36
37 resulted in a more pronounced acetylation of the microtubule network with enhanced process
38
39 elongation than sole enzymatic inhibition by **3b** (Fig 6, for raw images, see Supporting
40
41 Information, Fig. S4). By means of these studies we were able to show a successful example for
42
43 the envisaged superiority of the PROTAC concept with its extended target coverage over
44
45 occupancy-driven enzymatic inhibition.
46
47
48
49
50
51
52
53
54
55
56
57
58
59
60

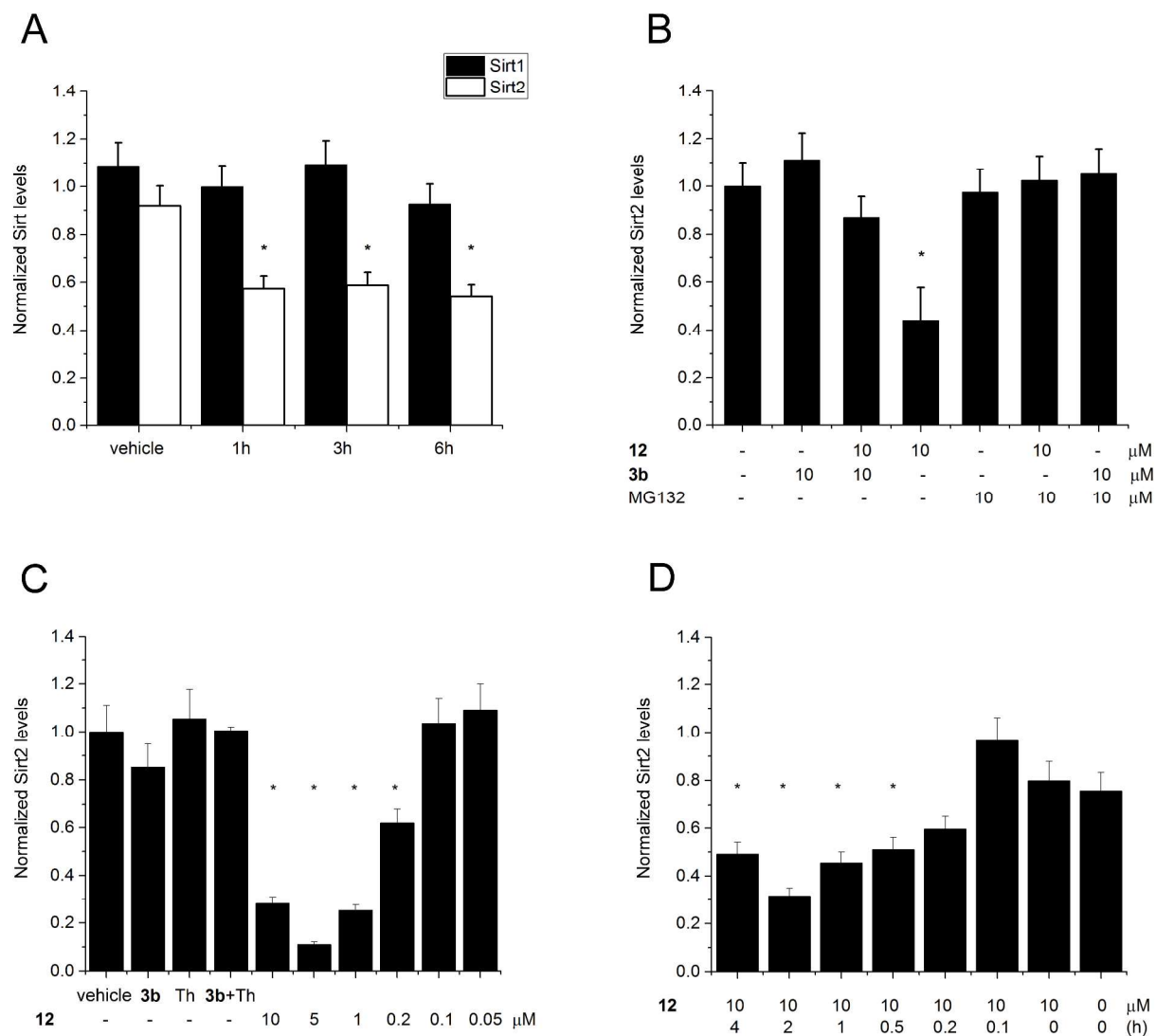
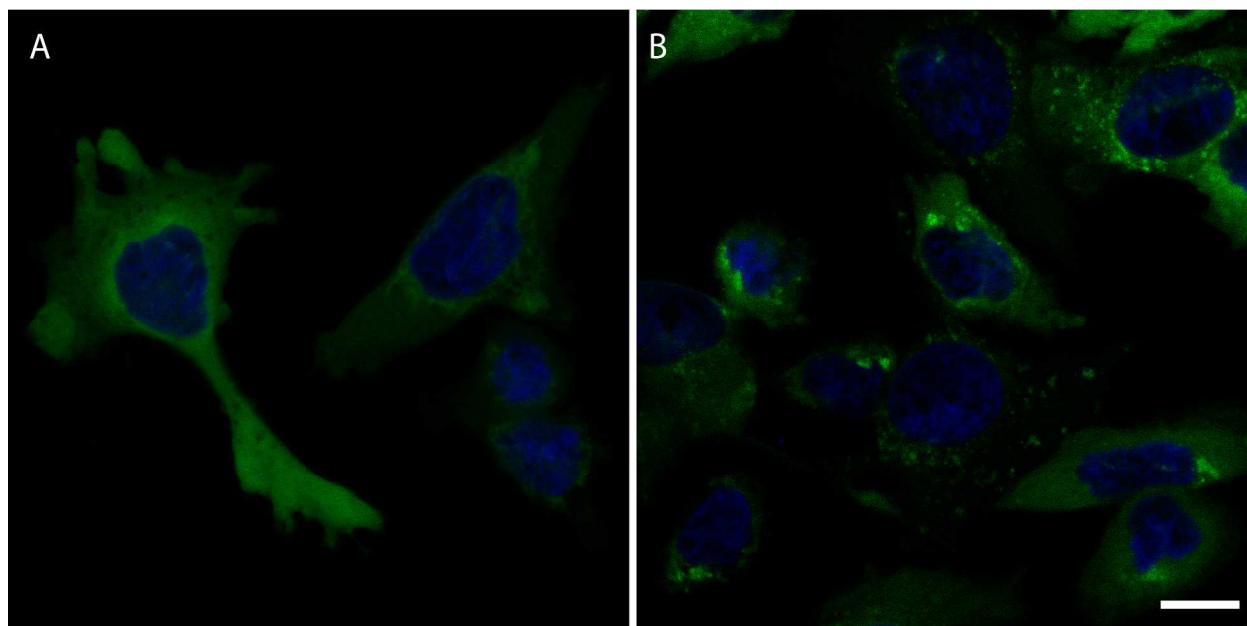
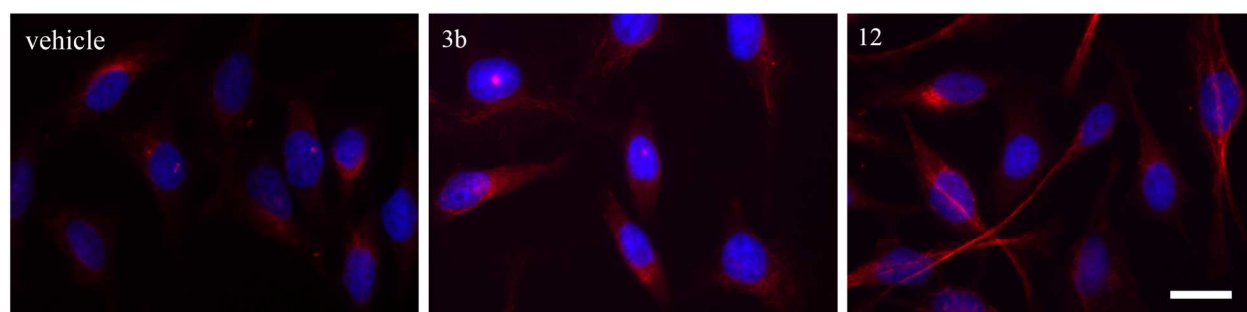


Figure 4. Quantification of the effect of **12** on the intracellular Sirt levels in HeLa cells by Western blot analyses. (A) Treatment with **12** (10 μ M) is able to chemically induce Sirt2 degradation. Sirt1 levels are not affected (n = 3). (B) The effect of **12** on the Sirt2 level in HeLa cells expressing EGFP-Sirt2 in the absence and presence of the proteasome inhibitor MG132 (n = 3). (C) Depletion of Sirt2 is dependent on the concentration of **12**. Control experiments with **3b** and thalidomide (Th) showed no significant effects on cellular Sirt2 levels, neither in single treatment nor in combination (n = 3). (D) Time course of Sirt2 depletion induced by **12** (n = 3).

1
2
3 Representative Western blots can be found in the Supporting Information (Fig. S3). Statistics
4
5 (t-test): * $p \leq 0.05$
6
7



29
30
31 **Figure 5.** Effect of **12** on the level and distribution of EGFP-Sirt2 (green) in living HeLa cells as
32 visualized by fluorescence microscopy. (A) Homogeneous distribution of the labelled Sirt2
33 (green). (B) Reduced Sirt2 level in the **12**-treated cells with dot-like pattern of the fluorescence
34 signal. Nuclei are stained with Hoechst 33342 (blue). Bar: 10 μm .
35
36
37
38
39



52
53
54
55
56
57
58
59
60

Figure 6. In cultured HeLa cells, depletion of Sirt2 due to treatment with **12** results in a more pronounced acetylation of the microtubule network than sole enzymatic inhibition by **3b**. Acetylation level of the microtubule network (red) in the presence or absence of sirtuin inhibitor

1
2
3 **3b** and the SirReal-based PROTAC (**12**), respectively. Tests were performed at a compound
4
5 concentration of 10 μ M. Nuclei were DAPI-stained (blue). The scale bar represents 10 μ m.
6
7
8
9

10
11
12 Thus, **12** is suitable to induce Sirt2 degradation with concomitantly increased efficacy of
13
14 tubulin hyperacetylation and therefore is the first example of a PROTAC targeting an epigenetic
15
16 eraser protein.
17
18
19

20 21 DISCUSSION AND CONCLUSION 22 23

24
25 In this study, we report the structure-based development of a PROTAC for Sirt2. Based on
26
27 our previously published work on the sirtuin rearranging ligands (SirReals) and a SirReal-based
28
29 affinity probe, we developed a highly potent and isotype-selective probe, which is capable of
30
31 chemically inducing the degradation of Sirt2. While several PROTACs for epigenetic reader
32
33 proteins have been reported yet, this is the first example of a PROTAC targeting an epigenetic
34
35 eraser protein. Since the PROTAC concept offers several advantages compared to occupancy-
36
37 driven enzyme inhibitors or genetic ablation of the enzyme, our novel tool for Sirt2 will open up
38
39 new avenues to dissect the role of Sirt2 in biology and medicine. Moreover, with our azido-
40
41 thalidomide-conjugate (**11**) we provide a versatile cereblon ligand building block, ready to be
42
43 “clicked” to alkynylated ligands of other proteins. Given the broad functional group tolerance of
44
45 this type of chemistry⁴³ and the availability of alkyne derivatives for many targets that have been
46
47 used in a large variety of chemical biology studies, this technique will be amenable to a plethora
48
49 of different targets and inhibitors. Thus, our study will not only help to interrogate Sirt2 biology
50
51
52
53
54
55
56
57
58
59
60

1
2
3 and druggability on a new level but also will accelerate the development of novel PROTACs for
4
5 other enzymes.
6
7

8 9 EXPERIMENTAL SECTION

10
11
12 **1. Cloning, expression and purification of recombinant proteins:** Human Sirt1₁₃₃₋₇₄₇ was
13 expressed as a GST-tagged enzyme and purified as described previously.⁴⁴ Sirt2₅₆₋₃₅₆ and
14 Sirt3₁₁₈₋₃₉₅ were expressed and purified as described previously with minor modifications.²⁸
15 Sirt2₅₆₋₃₅₆ and Sirt3₁₁₈₋₃₉₅ were resuspended in lysis buffer (25 mM KH₂PO₄, 25 mM NaH₂PO₄,
16 400 mM NaCl, 5% (v/v) glycerol, 5 mM beta-mercaptoethanol, pH 8.0) and purified as described
17 with a final Superdex S75 26/60 gel filtration column (25 mM Hepes, 200 mM NaCl, 5 % (v/v)
18 glycerol, pH 8.0). Identity and purity of the produced enzymes was verified using SDS-PAGE.⁴⁵
19 Protein concentration was determined by the Bradford assay.⁴⁶ Deacetylase activity of sirtuin
20 isotypes was NAD⁺-dependent and could be inhibited by nicotinamide. The eukaryote EGFP-
21 Sirt2 plasmid was a generous gift from Brian J. North (Department of Genetics, Harvard Medical
22 School, Boston, Massachusetts, USA).
23
24
25
26
27
28
29
30
31
32
33
34
35
36
37
38
39

40 **2. In Vitro Testing:** Inhibition tests for Sirt1, Sirt2 and Sirt3 were performed with a high-
41 throughput fluorescence-based histone deacetylase assay, as previously established by Heltweg
42 et al.⁴¹ Human Sirt1₁₃₃₋₇₄₇, Sirt2₅₆₋₃₅₆ or human Sirt3₁₁₈₋₃₉₅ were mixed with assay buffer (50 mM
43 Tris, 137 mM NaCl, 2.7 mM KCl, pH 8.0), NAD⁺ (final assay concentration 500 μM), the
44 substrate Z-(Ac)Lys-AMC (ZMAL, final assay concentration 10,5 μM), the inhibitor dissolved
45 in DMSO at different concentrations or DMSO as a control (final DMSO concentration 5%
46 (v/v)). To assure initial state conditions, total substrate conversion of controls was adjusted to
47 approximately 15% - 30%. The assay was performed in 96-well plates with a reaction volume of
48
49
50
51
52
53
54
55
56
57
58
59
60

1
2
3 60 μL per well. All determinations were performed in triplicates. After an incubation of 4 h at
4
5 37 $^{\circ}\text{C}$ and 140 rpm, deacetylation was stopped by the addition of 60 μL of a solution containing
6
7 trypsin and nicotinamide (50 mM Tris, 100 mM NaCl, 6.7% (v/v) DMSO, trypsin 5.5 U μL^{-1} ,
8
9 8 mM nicotinamide, pH 8.0). The microplate was further incubated for 20 min at 37 $^{\circ}\text{C}$ and 140
10
11 rpm. Fluorescence intensity was measured in a microplate reader (BMG Polarstar, $\lambda_{\text{ex}} = 390$ nm,
12
13 $\lambda_{\text{em}} = 460$ nm). Rates of inhibition were calculated by using the controls, containing no inhibitor,
14
15 as a reference. Graphpad Prism software (La Jolla, CA) was employed to determine IC_{50} values.
16
17
18
19

20
21 **3. Cell Culture:** HeLa (ATCC-2) cells were cultured in Dulbecco's Modified Eagle's Medium
22
23 (high glucose) supplemented with 10% (v/v) fetal calf serum, 100 $\mu\text{g}/\text{mL}$ kanamycin (all
24
25 reagents from Sigma, complete medium) in a humidified incubator at 37 $^{\circ}\text{C}$ with 5% CO_2 . For
26
27 immunoblotting of endogenous Sirt2 and Sirt1, 2×10^5 cells were plated in 6-well plates. A stable
28
29 EGFP-Sirt2 expressing cell population was generated by transfection of 10^6 HeLa cell with
30
31 Turbofect (Thermo Fisher) and EGFP-Sirt2 plasmid in 6 cm diameter petri dish according to the
32
33 manufacturer's protocol. Next day, the cells were selected by using 500 $\mu\text{g}/\text{mL}$ G418 for
34
35 4 weeks. Batches of this cell population were frozen for further work. For immunoblotting,
36
37 2×10^4 EGFP-Sirt2-HeLa cells were plated onto 24-well plates. Before adding compounds from
38
39 DMSO stocks, cycloheximide protein synthesis block was applied on cells (5 $\mu\text{g}/\text{ml}$ on 6-well
40
41 plates, 3 $\mu\text{g}/\text{ml}$ on 24-well plates) to detect degradation more effectively. For live microscopic
42
43 analysis, from the EGFP-Sirt2 expressing cell population, 2×10^4 cells were seeded onto the glass
44
45 based middle of 35 mm diameter imaging dishes 1.0 (Mo Bi Tec, Germany) in 1.0 mL complete
46
47 medium and incubated overnight. **12** (10 μM) was added into the dish to the treatment of cells,
48
49 which were incubated for the given incubation time. Unless otherwise stated, we chose an
50
51 incubation time of 4 hours. Next the complete medium was changed to a phenol red-free one
52
53
54
55
56
57
58
59
60

1
2
3 (Dulbecco's Modified Eagle's Medium, Sigma, D5921). Control cells were treated by DMSO
4
5 only. Live cell images were acquired with a Zeiss LSCM 710 microscope using an oiled 40× NA
6
7 = 1.4 Plan Apo objective. Nuclei were stained by 0.5 μg/mL Hoechst 33342 for 5 minutes.
8
9 Controls contained the corresponding amount of vehicle (DMSO).
10
11

12
13
14 **4. Immunoblotting:** For the detection of Sirt2, Sirt1 or glyceraldehyde-3-phosphate
15
16 dehydrogenase (GAPDH) levels in cellular samples, we kept the cells at 37 °C and washed them
17
18 with pre-warmed PBS. Next, the cells were lysed in 100 (24-well plate) or 300 (6-well plate) μL
19
20 1× reducing sample buffer containing protein inhibitor mix and 2 mM EDTA (Sigma-Aldrich) *in*
21
22 *situ*. Samples were centrifuged at 10000g at 4 °C for 5 min, and the supernatants were stored at
23
24 −70 °C. Samples were analyzed by 10% SDS-PAGE and blotted onto polyvinylidene difluoride
25
26 membrane (Millipore). The blot was developed sequentially using a rabbit antibody against Sirt2
27
28 (1:5000, affinity-isolated abcam ab67299, or RabMab ab51023), then using an affinity-isolated
29
30 rabbit antibody against Sirt1 (1:5000, Sigma, S5447) or using an affinity-isolated rabbit antibody
31
32 against GAPDH (1:5000, Sigma, G9545). Sirt1 could not be detected in the case of 24-well
33
34 samples, here GAPDH was used as loading control. Antibodies were detected by polyclonal anti-
35
36 rabbit IgG-peroxidase conjugate, (1:5000, Thermo Scientific). Peroxidase reaction was detected
37
38 using Immobilon Western substrate (Millipore) by a Bio-Rad ChemiDoc MP Imaging system
39
40 and its ImageLab 4.1 software. Intensity of spots was analyzed by ImageJ 1.49 using Measure
41
42 command and subtracting background values. The intensities were normalized by the average of
43
44 control values.
45
46
47
48
49
50

51
52
53 **5. Immunofluorescence Microscopy:** Immunofluorescence microscopy was performed as
54
55 previously reported.²⁸
56
57
58
59
60

1
2
3 **6. Computational Methods:** The following Sirt2 X-ray structures were used in the current
4 work: human Sirt2-SirReal-triazole probe (PDB ID 5DY5)^{29b} and human DDB1-CRBN E3
5 ubiquitin ligase-thalidomide (PDB ID 4CI2).³⁷ All protein structures were prepared by using the
6 Structure Preparation module in MOE 2012.10 (Chemical Computing Group, Montreal, Canada).
7
8 Hydrogen atoms were added, for titratable amino acids the protonation state was calculated using
9 the Protonate 3D module in MOE 2012.10. Water molecules and ligand atoms except the zinc
10 ion and one conserved water molecule bound to Sirt2 Pro94 were removed from the structures.

11
12
13
14
15
16
17
18
19
20
21 To generate the Sirt2-cereblon complexes the protein-protein docking program HADDOCK
22 (version 2.2) was used.³⁶ HADDOCK uses an initial rigid-body docking process which generates
23 typically a large number of structures in the order of thousands. From these a number of
24 structures, typically several hundred, are selected for further flexible refinement and scoring
25 using HADDOCK score, van-der-Waals and electrostatic interactions. The following residues
26 located at the entrance of both binding pockets were chosen to define the protein-protein
27 interaction site: Ser100, Phe235, Ser263, Ile300 for Sirt2, Gln86, His103, Phe150, Thr376 for
28 cereblon. HADDOCK calculated eleven different clusters for the Sirt2-cereblon complex. Among
29 the eleven complexes the three best scored complexes were chosen for further analysis and
30 ligand docking studies. The results of the HADDOCK protein-protein docking are provided in
31 the Supplementary Information (Figure S1). Docking studies were performed using program
32 GOLD (version 5.2) and GoldScore.⁴⁷ From each of the three protein-protein clusters provided
33 by HADDOCK, four complexes were chosen for the docking study. The backbone carbonyl
34 oxygen of Sirt2-Phe235 was defined as center of the binding site with 20 Å radius. 50 docking
35 poses were calculated for the ligand. All other options were left at their default values. The
36 retained docking poses were further refined using a MM-GBSA protocol. The AMBEREHT12
37
38
39
40
41
42
43
44
45
46
47
48
49
50
51
52
53
54
55
56
57
58
59
60

1
2
3 force field and the GBSA method implemented in MOE 2012.10 were used to relax the protein-
4 inhibitor complexes. During the minimization protein backbone atoms were tethered using a
5 force constant of $(3/2) kT / 2$ ($\sigma = 0.5 \text{ \AA}$).⁴⁸ Complexes showing the lowest binding free energies
6 values were selected. The docking protocol has already been successfully applied in case of
7 Sirt2.²⁹ For cereblon (PDB ID 4CI2)³⁷ GOLD was correctly reproducing the binding mode of
8 thalidomide with an RMSD value of 0.45 \AA .
9
10
11
12
13
14
15
16

17
18 **7. Chemistry:** Starting materials and reagents were obtained from commercial suppliers and
19 used without further purification. Thin-layer chromatography (TLC) for reaction monitoring was
20 performed with alumina plates coated with Merck silica gel 60 F₂₅₄ (layer thickness: 0.2 mm)
21 and analyzed under UV-light (254 nm). The composition of the mobile phase was adjusted to
22 compound properties. Yields were not optimized. ¹H NMR and ¹³C NMR spectra were recorded
23 on Bruker Avance III HD spectrometer at 400 MHz and 100 MHz. The spectra are referenced
24 against the NMR solvents and are reported as follows: ¹H: chemical shift δ (ppm), multiplicity (s
25 = singlet, d = doublet, dd = doublet of doublets, t = triplet, q = quartet, quint = quintet, sex =
26 sextet, m = multiplet, b = broad), integration, coupling constant (J in Hz). ¹³C: chemical shift δ
27 (ppm), abbreviations: (q) = quaternary carbons, quaternary carbons that could not be found in ¹³C
28 spectra but in HMBC or HSQC are additionally marked with an asterisk (*). ¹H or ¹³C signals
29 that are partially overlapping with solvent residual signals are marked with a hashtag (#). The
30 assignment resulted from HMBC and HSQC experiments. Purity of the tested compound was
31 determined by HPLC and UV detection ($\lambda = 210 \text{ nm}$) and was > 95%. HPLC analysis was
32 performed using the following conditions: Eluent A: H₂O containing 0.05% TFA, Eluent B:
33 acetonitrile containing 0.05% TFA, flow rate 1 mL min⁻¹, linear gradient conditions (0–4 min, A
34 = 90%, B = 10%; 4–29 min, linear increase to 100 % of B; 29–31 min, B = 100%; 31–40 min, A
35
36
37
38
39
40
41
42
43
44
45
46
47
48
49
50
51
52
53
54
55
56
57
58
59
60

1
2
3 = 10%, B = 90%), Merk LiChrospher 60 RP-select B (5 μm , 60 \AA , 250 x 4 mm) as an analytical
4
5
6 column. Melting temperatures were determined in glass capillary tubes with the Stuart Melting
7
8 Point Apparatus SMP2. Mass spectra with electrospray ionization (ESI) were recorded on an
9
10 Advion expression CMS spectrometer or on a Exactive device (Thermo Fisher Scientific, for
11
12 FTMS). The synthesis of compounds **6** and **8** has already been reported.³⁸⁻³⁹ Due to changes in
13
14 the experimental procedure and to show unpublished characterization data, we have outlined the
15
16 synthesis and the characterization data for those compound as well.
17
18
19

20
21 Dimethyl 3-hydroxyphthalate (**6**). From 3-hydroxyphthalic acid anhydride (**5**) according to a
22
23 modified procedure published by Kristiansen et al.³⁸ Thionyl chloride (5 equiv) was added
24
25 dropwise to an ice-cold solution of 3-hydroxyphthalic acid anhydride (1 equiv, 3.7 mmol) in
26
27 methanol (10 mL). Then, the mixture was stirred for 4 h at 80 °C under reflux conditions. After
28
29 completion, solvents were removed under reduced pressure. The remaining crude product was
30
31 purified by automated flash chromatography (cyclohexane/EtOAc: gradient 10% - 100%
32
33 EtOAc). Yield, 63% of a colorless solid; R_f , 0.46 (cyclohexane/EtOAc, 7:3 (v/v)); ^1H NMR
34
35 (DMSO- d_6 , δ [ppm]): 10.34 (s, 1H, -O-H), 7.41-7.36 (m, 2H, H-5,6), 7.18-7.14 (m, 1H, H-4),
36
37 3.80 (s, 3H, -COO-CH₃ at C-1), 3.77 (s, 3H, -COO-CH₃ at C-2). ^{13}C NMR (DMSO- d_6 , δ [ppm]):
38
39 167.57 q (-COO-CH₃ at C-2), 166.02 q (-COO-CH₃ at C-1), 154.96 q (C-3), 130.93 (C-5),
40
41 128.86 q (C-1), 122.96 q (C- 2), 120.85 (C-4), 120.36 (C-6), 52.89 (-COO-CH₃ at C-1), 52.50
42
43 (-COO-CH₃ at C-2). ESI-MS(-): 209.2 [M - H]⁻.
44
45
46
47
48
49

50
51 4-Azidobutan-1-aminium chloride (**8**).³⁹ From *N*-(4-bromobutyl)phthalimide (**7**) according to a
52
53 modified procedure published by Cunningham et al.³⁹ **7** (1 equiv, 9.9 mmol) was dissolved in
54
55 DMF (20 mL). After the addition of NaN₃ (1.1 equiv) the reaction mixture was stirred for 12 h at
56
57 ambient temperature. Water (25 mL) was added and the aqueous layer was extracted with EtOAc
58
59
60

(30 mL, three times). The organic layers were dried over MgSO_4 and evaporated. The residue was dissolved in ethanol (40 mL). The solution was cooled to 0 °C and hydrazine monohydrate (2 equiv) was gradually added in portions while stirring. Then, the mixture was stirred for 24 h at ambient temperature. After completion, the reaction mixture was acidified with concentrated hydrochloric acid. Solvents were evaporated under reduced pressure and water (30 mL) was added to the residue. Potassium hydroxide was added to adjust a basic pH value ($\text{pH} > 10$). The aqueous layer was extracted with dichloromethane (30 mL, four times). The combined organic layers were dried over MgSO_4 , acidified with concentrated hydrochloric acid, and evaporated under reduced pressure. Yield, > 99% of a colorless oil; ^1H NMR ($\text{DMSO-}d_6$, δ [ppm]): 8.10 (bs, 3H, H_3N^+ -), 3.37 (t, 2H, $^3\text{J} = 6.45$ Hz, $\text{H}_3\text{N}^+\text{-CH}_2\text{-CH}_2\text{-CH}_2\text{-CH}_2\text{-N}_3$), 2.78 (sex, 2H, $^3\text{J} = 6.33$ Hz, $\text{H}_3\text{N}^+\text{-CH}_2\text{-CH}_2\text{-CH}_2\text{-CH}_2\text{-N}_3$), 1.69-1.51 (m, 4H, $\text{H}_3\text{N}^+\text{-CH}_2\text{-CH}_2\text{-CH}_2\text{-CH}_2\text{-N}_3$). ^{13}C NMR ($\text{DMSO-}d_6$, δ [ppm]): 50.52 ($\text{H}_3\text{N}^+\text{-CH}_2\text{-CH}_2\text{-CH}_2\text{-CH}_2\text{-N}_3$), 38.60 ($\text{H}_3\text{N}^+\text{-CH}_2\text{-CH}_2\text{-CH}_2\text{-CH}_2\text{-N}_3$), 25.74 ($\text{H}_3\text{N}^+\text{-CH}_2\text{-CH}_2\text{-CH}_2\text{-CH}_2\text{-N}_3$), 24.69 ($\text{H}_3\text{N}^+\text{-CH}_2\text{-CH}_2\text{-CH}_2\text{-CH}_2\text{-N}_3$). ESI-MS(+): 115.2 [$\text{M} - \text{Cl}$] $^+$.

N-(4-azidobutyl)-2-chloroacetamide (**9**). **8** (1equiv, 9.7 mmol) was dissolved in DMF (15 mL) and trimethylamine (2 equiv) was added. The mixture was cooled to 0 °C and chloroacetyl chloride was gradually added. The reaction mixture was stirred for 10 min at 0 °C and then for further 60 min at ambient temperature. After the addition of a saturated aqueous solution of sodium bicarbonate (30 mL) the mixture was extracted with EtOAc (30 mL, three times). The combined organic layers were dried over MgSO_4 and evaporated under reduced pressure. Yield, 82% of a yellowish oil; ^1H NMR ($\text{DMSO-}d_6$, δ [ppm]): 8.33-8.15 (m, 1H, amide-H), 4.04 (s, 2H, $\text{Cl-CH}_2\text{-CO-NH-}$), 3.34 $^\#$ (t, 2H, $^3\text{J} = 6.64$ Hz, $\text{-CH}_2\text{-CH}_2\text{-N}_3$), 3.11 (q, 2H, $^3\text{J} = 6.31$, $\text{-CO-NH-CH}_2\text{-CH}_2\text{-}$), 1.60-1.40 (m, 4H, $\text{-CO-NH-CH}_2\text{-CH}_2\text{-CH}_2\text{-CH}_2\text{-N}_3$). ^{13}C NMR

(DMSO-*d*₆, δ [ppm]): 166.25 (amide-C), 50.71 (-CH₂-N₃), 43.08 (Cl-CH₂-CO-NH-), 38.75 (-CO-NH-CH₂-), 26.52 (-CO-NH-CH₂-CH₂-), 26.09 (-CH₂-CH₂-N₃). FTMS(+): 191.0693 [M + H]⁺.

Dimethyl 3-(2-((4-azidobutyl)amino)-2-oxoethoxy)phthalate (**10**). **7** (1 equiv, 2.1 mmol) and **9** (1.1 equiv) were dissolved in acetonitrile (20 mL) and Cs₂CO₃ (2 equiv) was added. The reaction mixture was stirred for 5 h at 60 °C under reflux conditions and for further 12 h at ambient temperature. Water (15 mL) was added to the reaction mixture and the aqueous layer was extracted with dichloromethane (15 mL, once) and EtOAc (20 mL, three times). The combined organic layers were dried over MgSO₄ and evaporated under reduced pressure. The remaining crude product was purified by automated flash chromatography (cyclohexane/EtOAc: gradient 10% - 100% EtOAc). Yield, 88% of a colorless oil; *R*_f, 0.33 (cyclohexane/EtOAc, 6:4 (v/v)); ¹H NMR (DMSO-*d*₆, δ [ppm]): 7.80 (t, 1H, ³J = 6.04 Hz, amide-H), 7.59-7.53 (m, 2H, phthalate H-5,6), 7.38-7.31 (m, 1H, phthalate H-4), 4.62 (s, 2H, -O-CH₂-CO-NH-), 3.85-3.80 (m, 6H, -COO-CH₃), 3.33[#] (t, 2H, ³J = 6.12 Hz, -CH₂-CH₂-N₃), 3.16 (q, 2H, ³J = 6.04 Hz, -CO-NH-CH₂-CH₂), 1.52-1.47 (m, 4H, -CO-NH-CH₂-CH₂-CH₂-CH₂-N₃). ¹³C NMR (DMSO-*d*₆, δ [ppm]): 167.35 q (amide-C), 167.13 q (-COO-CH₃ at phthalate C-2), 165.59 q (-COO-CH₃ at phthalate C-1), 155.21 q (phthalate C-3), 131.44 (phthalate C-5), 129.01 q (phthalate C-1), 124.81 q (phthalate C-2), 122.60 (phthalate C-6), 118.38 (phthalate C-4), 68.35 (O-CH₂-CO-NH-), 53.13 (-COO-CH₃ at phthalate C-1), 52.90 (-COO-CH₃ at phthalate C-2), 50.71 (-CH₂-N₃), 38.16 (-CO-NH-CH₂-), 26.63 & 26.05 (-CO-NH-CH₂-CH₂-CH₂-CH₂-N₃). ESI-MS(+): 387.1 [M + Na]⁺.

N-(4-azidobutyl)-2-((2-(2,6-dioxopiperidin-3-yl)-1,3-dioxoisindolin-4-yl)oxy)acetamide (**11**): **10** (1 equiv, 1.85 mmol) was dissolved in ethanol (15 mL) and an aqueous sodium hydroxide solution (2.5 equiv, 3 M) was added. The reaction mixture was stirred for 1.5 h at ambient

1
2
3 temperature. Subsequently, solvents were evaporated under reduced pressure and the residue was
4 dissolved in water (15 mL). The aqueous layer was washed with EtOAc. The organic layer was
5 discarded and the aqueous layer was acidified with diluted hydrochloric acid and extracted with
6 EtOAc (20 mL, three times). The combined organic layers were dried over MgSO₄ and
7 evaporated under reduced pressure. The crude dicarboxylic acid, 3-aminopiperidine-2,6-dione
8 hydrochloride (1.2 equiv), *N,N*-dimethylpyridin-4-amine (0.2 equiv), and trimethylamine (3.4
9 equiv) were dissolved in dichloromethane (15 mL). The mixture was cooled to 0 °C and
10 *N,N'*-dicyclohexylcarbodiimide was added under nitrogen atmosphere. After 15 min of stirring at
11 0 °C the reaction mixture was stirred for further 22 h at ambient temperature. The precipitate was
12 separated by filtration was dried under reduced pressure. The crude product was purified by
13 automated flash chromatography (dichloromethane/methanol: gradient 1% - 10% methanol).
14 Yield, 50% of a white solid; mp, 165 °C; *R*_f, 0.71 (dichloromethane/methanol, 19:1 (v/v));
15 ¹H NMR (DMSO-*d*₆, δ [ppm]): 11.14 (bs, 1H, -CO-NH-CO-), 8.03 (t, 1H, ³J = 6.04 Hz,
16 amide-H), 7.82 (dd, 1H, ³J = 8.59 Hz, ³J = 7.33 Hz, 1,3-dioxoisindoline H-6), 7.51 (d, 1H, ³J =
17 7.33 Hz, 1,3-dioxoisindoline H-7), 7.40 (d, 1H, ³J = 8.59 Hz, 1,3-dioxoisindoline H-5), 5.13
18 (dd, 1H ³J = 12.87 Hz, ³J = 5.43 Hz, 1H, 2,6-dioxopiperidine H-3), 4.79 (s,
19 2H, -O-CH₂-CO-NH-), 3.34[#] (t, 2H, ³J = 6.55 Hz, -CH₂-CH₂-N₃), 3.17 (q, 2H, ³J = 6.04
20 Hz, -CO-NH-CH₂-CH₂), 2.95-2.86 (m, 1H, 2,6-dioxopiperidine H-4), 2.63-2.53[#] (m, 2H,
21 2,6-dioxopiperidine H-5), 2.06-2.03 (m, 1H, 2,6-dioxopiperidine H-4), 1.58-1.44 (m,
22 4H, -CO-NH-CH₂-CH₂-CH₂-CH₂-N₃). ¹³C NMR (DMSO-*d*₆, δ [ppm]): 173.21 q
23 (2,6-dioxopiperidine C-6), 170.31 q (2,6-dioxopiperidine C-2), 167.19 q (amide-C), 167.15 q
24 (1,3-dioxoisindoline C-1), 165.92 q (1,3-dioxoisindoline C-3), 155.49 q (1,3-dioxoisindoline
25 C-4), 137.35 (1,3-dioxoisindoline C-6), 133.45 q (1,3-dioxoisindoline C-7a), 120.80
26
27
28
29
30
31
32
33
34
35
36
37
38
39
40
41
42
43
44
45
46
47
48
49
50
51
52
53
54
55
56
57
58
59
60

1
2
3 (1,3-dioxoisindoline C-5), 117.23 (1,3-dioxoisindoline C-3a), 116.48 (1,3-dioxoisindoline
4 C-7), 68.07 (-O-CH₂-CO-NH-), 50.71 (-CH₂-N₃), 49.20 (2,6-dioxopiperidine C-3), 38.20
5
6 (-CO-NH-CH₂-), 31.36 (2,6-dioxopiperidine C-5), 26.67 & 26.08 (-CO-NH-CH₂-CH₂-CH₂-CH₂-
7
8 N₃), 22.39 (2,6-dioxopiperidine C-4). ESI-MS(-): 427.2 [M - H]⁻.
9

10
11
12
13
14 2-((4,6-dimethylpyrimidin-2-yl)thio)-N-(5-(3-((1-(4-(2-((2-(2,6-dioxopiperidin-3-yl)-1,3-
15
16 dioxoisindolin-4-yl)oxy)acetamido)butyl)-1H-1,2,3-triazol-4-yl)methoxy)benzyl)thiazol-2-
17
18 yl)acetamide (**12**): **11** (1 equiv, 0.47 mmol) and **2** (1 equiv) were suspended in a water/*tert*-
19
20 butanol mixture (10 mL, 1:1). The suspension was sonified for 15 min. An aqueous CuSO₄
21
22 solution (0.2 equiv, 0.1 M) and an aqueous solution of sodium ascorbate (0.4 equiv, 0.1 M) were
23
24 added in that order. The resulting reaction mixture was stirred for 1h at 60 °C and for further
25
26 16 h at ambient temperature under nitrogen atmosphere. After completion the reaction was
27
28 quenched by the addition of water (15 mL). The aqueous layer was extracted with
29
30 dichloromethane (30 mL, three times) and the combined organic layers were dried over MgSO₄
31
32 and evaporated under reduced pressure. The remaining crude product was purified by automated
33
34 flash chromatography (dichloromethane/methanol: gradient 1% - 10% methanol). Finally, the
35
36 product was recrystallized from methanol. Yield, 33% of a white solid; mp, 135 °C; *R*_f, 0.25
37
38 (dichloromethane/methanol, 19:1 (v/v)); ¹H NMR (DMSO-*d*₆, δ [ppm]): 12.22 (bs,
39
40 1H, -NH-CO-CH₂-S-), 11.13 (bs, 1H, -CO-NH-CO-), 8.19 (s, 1H, triazole-H), 8.03 (t, 1H, ³J =
41
42 5.82 Hz, -NH-CO-CH₂-O-), 7.79 (dd, 1H, ³J = 8.44 Hz, ³J = 7.36 Hz, 1,3-dioxoisindoline H-6),
43
44 7.48 (d, 1H, ³J = 7.36 Hz, 1,3-dioxoisindoline H-7), 7.37 (d, 1H, ³J = 8.44 Hz,
45
46 1,3-dioxoisindoline H-5), 7.27-7.20 (m, 2H, thiazole H-4 & phenyl H-5), 6.94 (s, 1H,
47
48 pyrimidine H-5), 6.92-6.87 (m, 2H, phenyl H-2,4), 6.84 (d, 1H, ³J = 7.51 Hz, phenyl H-6),
49
50 5.16-5.09 (m, 3H, 2,6-dioxopiperidine H-3 & triazole-CH₂-O-), 4.78 (s, 2H, -O-CH₂-CO-NH-),
51
52
53
54
55
56
57
58
59
60

1
2
3 4.37 (t, 2H, $^3J = 7.00$ Hz, $-\text{CH}_2-\underline{\text{CH}_2}$ -triazole), 4.08[#] (s, 2H, $-\text{NH}-\text{CO}-\underline{\text{CH}_2}$ -S-), 4.04 (s, 2H,
4 thiazole- CH_2 -phenyl), 3.21-3.12[#] (m, 2H, $-\text{CH}_2-\underline{\text{CH}_2}$ -NH-CO-), 2.96-2.79 (m, 1H,
5 2,6-dioxopiperidine H-4), 2.65-2.53[#] (m, 2H, 2,6-dioxopiperidine H-5), 2.28 (s, 6H,
6 pyrimidine $-\text{CH}_3$), 2.09-2.00 (m, 1H, 2,6-dioxopiperidine H-4), 1.86-1.73 (m, 2H, $-\text{CO}-\text{NH}-\text{CH}_2$ -
7 $\text{CH}_2-\underline{\text{CH}_2}$ - CH_2 -triazole), 1.46-1.35 (m, 2H, $-\text{CO}-\text{NH}-\text{CH}_2-\underline{\text{CH}_2}$ - CH_2-CH_2 -triazole) . ^{13}C NMR
8 (DMSO- d_6 , δ [ppm]): 172.85 q (2,6-dioxopiperidine C-6), 169.91 q (2,6-dioxopiperidine C-2),
9 168.91 q (pyrimidine C-2), 167.02 q (pyrimidine C-4,6), 166.84 q ($-\text{NH}-\underline{\text{CO}}-\text{CH}_2$ -S- & $-\text{NH}-\underline{\text{CO}}-$
10 CH_2 -O-), 166.75 q (1,3-dioxoisindoline C-1), 165.50 q (1,3-dioxoisindoline C-3), 158.21 q
11 (phenyl C-3), 156.91 q (thiazole C-2), 155.11 q (1,3-dioxoisindoline C-4), 142.61 q (triazole
12 C-4), 141.90 q (phenyl C-1), 136.93 (1,3-dioxoisindoline C-6), 134.79 (thiazole C-4), 133.05 q
13 (1,3-dioxoisindoline C-7a), 131.07 q (thiazole C-5), 129.66 (phenyl C-5), 124.37 (triazole C-5),
14 120.92 (phenyl C-6), 120.37 (1,3-dioxoisindoline C-5), 116.82 (1,3-dioxoisindoline C-3a),
15 116.13 (pyrimidine C-5), 116.05 (1,3-dioxoisindoline C-7), 114.95 (phenyl C-2), 112.44
16 (phenyl C-4), 67.65 ($\text{O}-\underline{\text{CH}_2}$ -CO-NH-), 61.06 ($-\text{O}-\text{CH}_2$ -triazole), 49.01 (triazole- CH_2 -), 48.81
17 (2,6-dioxopiperidine C-3), 37.66 ($-\text{CO}-\text{NH}-\underline{\text{CH}_2}$ -), 34.07 ($-\text{NH}-\text{CO}-\underline{\text{CH}_2}$ -S-), 31.90
18 (thiazole- CH_2 -phenyl), 30.96 (2,6-dioxopiperidine C-5), 27.15 ($-\text{CO}-\text{NH}-\text{CH}_2-\text{CH}_2-\underline{\text{CH}_2}$ - CH_2 -
19 triazole), 26.02 ($-\text{CO}-\text{NH}-\text{CH}_2-\underline{\text{CH}_2}$ - CH_2-CH_2 -triazole), 23.26 (pyrimidine $-\text{CH}_3$), 22.00
20 (2,6-dioxopiperidine C-4). Purity: 97.7% (18.8 min). ESI-MS(-): 851.9 [M - H]⁻.
21
22
23
24
25
26
27
28
29
30
31
32
33
34
35
36
37
38
39
40
41
42
43
44
45
46

47 **8. PAINS Analysis:** Moreover, we assessed whether the compounds possessed any structural
48 features which should render them pan-assay-interferers by applying the PAINS filter.⁴⁹
49 Screening against PAINS was performed using the program KNIME,⁵⁰ using a workflow
50 downloaded from <http://www.myexperiment.org/workflows/1841.html>.⁵¹ The target molecule **12**
51
52
53
54
55
56
57
58
59
60

1
2
3 is not identified as a potential PAINS. Intermediates **8-11** are flagged due the azide function
4
5 (contain an azo group) but are only used in synthesis and are not evaluated in biological assays.
6
7
8
9
10

11 12 13 14 15 ASSOCIATED CONTENT

16
17
18
19 **Supporting Information.** The Supporting Information is available free of charge on ACS
20
21 Publications website at DOI:

22
23
24
25 Supplementary Figures: Fig S1–4 (PDF)

26
27
28 Molecular formular strings (CSV)

29 30 31 AUTHOR INFORMATION

32 33 34 **Corresponding Author**

35
36
37 *Phone: +497612034896. Fax: +497612036321. E-mail: manfred.jung@pharmazie.uni-
38
39 freiburg.de

40 41 42 **Present Addresses**

43
44
45 ∇ Matthias Schiedel: Department of Chemistry, Chemistry Research Laboratory, University of
46
47 Oxford, Mansfield Road, OX1 3TA Oxford, United Kingdom

48 49 50 **Author Contributions**

51
52
53 The manuscript was written through contributions of all authors. All authors have given approval
54
55 to the final version of the manuscript.
56
57
58
59
60

Notes

The authors declare no competing financial interest.

ACKNOWLEDGMENT

We thank the Deutsche Forschungsgemeinschaft (DFG) for funding (INST 39/931-1 and CRC992 to M.J., Ju 295-13/1 to D.H. and M.J.). This work was supported by the European Concerted Research Action COST Action EPICHEMPIO [CM1406]; and Hungarian National Scientific Research Fund Grants OTKA [K-101039 and K-112144] to J. O.

ABBREVIATIONS

AMC, 7-Amino-4-methylcoumarin; BubR1, budding uninhibited by benzimidazoles related 1 protein; EGFP, enhanced green fluorescent protein; EtOAc, ethyl acetate; HOXA10, Hoxa10 homeobox A10 protein; KDAC, lysine deacetylase; NF κ B, nuclear factor 'kappa-light-chain-enhancer' of activated B-cells; p53, tumor suppressor protein p53; POI, protein of interest; PROTAC, proteolysis targeting chimera; SirReal, sirtuin rearranging ligand; SMILES, simplified molecular input line entry specification; VHL, Von Hippel–Lindau tumor suppressor; ZMAL, Z-(Ac)Lys-AMC

Authors will release the atomic coordinates of the protein-protein docking model upon article publication.

REFERENCES

1. de Ruijter, A. J.; van Gennip, A. H.; Caron, H. N.; Kemp, S.; van Kuilenburg, A. B. Histone deacetylases (HDACs): characterization of the classical HDAC family. *Biochem. J.* **2003**, *370*, 737-749.
2. Imai, S.; Armstrong, C. M.; Kaeberlein, M.; Guarente, L. Transcriptional silencing and longevity protein Sir2 is an NAD-dependent histone deacetylase. *Nature* **2000**, *403*, 795-800.
3. (a) Schemies, J.; Uciechowska, U.; Sippl, W.; Jung, M. NAD(+) -dependent histone deacetylases (sirtuins) as novel therapeutic targets. *Med. Res. Rev.* **2010**, *30*, 861-889; (b) Schiedel, M.; Robaa, D.; Rumpf, T.; Sippl, W.; Jung, M. The current state of NAD⁺ -dependent histone deacetylases (sirtuins) as novel therapeutic targets. *Med. Res. Rev.* **2017**, [Online early access]. DOI: 10.1002/med.21436. Published Online: January 17, 2017.
4. Bao, X.; Wang, Y.; Li, X.; Li, X. M.; Liu, Z.; Yang, T.; Wong, C. F.; Zhang, J.; Hao, Q.; Li, X. D. Identification of 'erasers' for lysine crotonylated histone marks using a chemical proteomics approach. *eLife* **2014**, *3*, e02999.
5. Tan, M. J.; Peng, C.; Anderson, K. A.; Chhoy, P.; Xie, Z. Y.; Dai, L. Z.; Park, J.; Chen, Y.; Huang, H.; Zhang, Y.; Ro, J.; Wagner, G. R.; Green, M. F.; Madsen, A. S.; Schmiesing, J.; Peterson, B. S.; Xu, G. F.; Ilkayeva, O. R.; Muehlbauer, M. J.; Braulke, T.; Muhlhausen, C.; Backos, D. S.; Olsen, C. A.; McGuire, P. J.; Pletcher, S. D.; Lombard, D. B.; Hirschey, M. D.; Zhao, Y. M. Lysine glutarylation is a protein posttranslational modification regulated by SIRT5. *Cell Metab.* **2014**, *19*, 605-617.

- 1
2
3
4
5
6
7
8
9
10
11
12
13
14
15
16
17
18
19
20
21
22
23
24
25
26
27
28
29
30
31
32
33
34
35
36
37
38
39
40
41
42
43
44
45
46
47
48
49
50
51
52
53
54
55
56
57
58
59
60
6. Du, J.; Zhou, Y.; Su, X.; Yu, J. J.; Khan, S.; Jiang, H.; Kim, J.; Woo, J.; Kim, J. H.; Choi, B. H.; He, B.; Chen, W.; Zhang, S.; Cerione, R. A.; Auwerx, J.; Hao, Q.; Lin, H. Sirt5 is a NAD-dependent protein lysine demalonylase and desuccinylase. *Science* **2011**, *334*, 806-809.
7. Feldman, J. L.; Baeza, J.; Denu, J. M. Activation of the protein deacetylase SIRT6 by long-chain fatty acids and widespread deacylation by mammalian sirtuins. *J. Biol. Chem.* **2013**, *288*, 31350-31356.
8. Jiang, H.; Khan, S.; Wang, Y.; Charron, G.; He, B.; Sebastian, C.; Du, J. T.; Kim, R.; Ge, E.; Mostoslavsky, R.; Hang, H. C.; Hao, Q.; Lin, H. N. SIRT6 regulates TNF-alpha secretion through hydrolysis of long-chain fatty acyl lysine. *Nature* **2013**, *496*, 110-113.
9. (a) Tong, Z.; Wang, Y.; Zhang, X.; Kim, D. D.; Sadhukhan, S.; Hao, Q.; Lin, H. SIRT7 is activated by DNA and deacetylates histone H3 in the chromatin context. *ACS Chem. Biol.* **2016**, *11*, 742-747; (b) Tong, Z.; Wang, M.; Wang, Y.; Kim, D. D.; Grenier, J. K.; Cao, J.; Sadhukhan, S.; Hao, Q.; Lin, H. SIRT7 is an RNA-activated protein lysine deacylase. *ACS Chem. Biol.* **2017**, *12*, 300-310.
10. North, B. J.; Marshall, B. L.; Borra, M. T.; Denu, J. M.; Verdin, E. The human Sir2 ortholog, SIRT2, is an NAD⁺-dependent tubulin deacetylase. *Mol. Cell* **2003**, *11*, 437-444.
11. Vaziri, H.; Dessain, S. K.; Ng Eaton, E.; Imai, S. I.; Frye, R. A.; Pandita, T. K.; Guarente, L.; Weinberg, R. A. hSIR2(SIRT1) functions as an NAD-dependent p53 deacetylase. *Cell* **2001**, *107*, 149-159.
12. North, B. J.; Rosenberg, M. A.; Jeganathan, K. B.; Hafner, A. V.; Michan, S.; Dai, J.; Baker, D. J.; Cen, Y.; Wu, L. E.; Sauve, A. A.; van Deursen, J. M.; Rosenzweig, A.; Sinclair, D. A. SIRT2 induces the checkpoint kinase BubR1 to increase lifespan. *EMBO J.* **2014**, *33*, 1438-1453.

- 1
2
3
4
5
6
7
8
9
10
11
12
13
14
15
16
17
18
19
20
21
22
23
24
25
26
27
28
29
30
31
32
33
34
35
36
37
38
39
40
41
42
43
44
45
46
47
48
49
50
51
52
53
54
55
56
57
58
59
60
13. Yeung, F.; Hoberg, J. E.; Ramsey, C. S.; Keller, M. D.; Jones, D. R.; Frye, R. A.; Mayo, M. W. Modulation of NF-kappaB-dependent transcription and cell survival by the SIRT1 deacetylase. *EMBO J.* **2004**, *23*, 2369-2380.
 14. Feige, J. N.; Auwerx, J. Transcriptional targets of sirtuins in the coordination of mammalian physiology. *Curr. Opin. Cell Biol.* **2008**, *20*, 303-309.
 15. Verdin, E.; Hirschey, M. D.; Finley, L. W.; Haigis, M. C. Sirtuin regulation of mitochondria: energy production, apoptosis, and signaling. *Trends Biochem. Sci.* **2010**, *35*, 669-675.
 16. Liu, T. F.; Vachharajani, V. T.; Yoza, B. K.; McCall, C. E. NAD⁺-dependent sirtuin 1 and 6 proteins coordinate a switch from glucose to fatty acid oxidation during the acute inflammatory response. *J. Biol. Chem.* **2012**, *287*, 25758-25769.
 17. Haigis, M. C.; Guarente, L. P. Mammalian sirtuins--emerging roles in physiology, aging, and calorie restriction. *Genes Dev.* **2006**, *20*, 2913-2921.
 18. de Oliveira, R. M.; Sarkander, J.; Kazantsev, A. G.; Outeiro, T. F. SIRT2 as a therapeutic target for age-related disorders. *Front. Pharmacol.* **2012**, *3*, 92-100.
 19. Beirowski, B.; Gustin, J.; Armour, S. M.; Yamamoto, H.; Viader, A.; North, B. J.; Michan, S.; Baloh, R. H.; Golden, J. P.; Schmidt, R. E.; Sinclair, D. A.; Auwerx, J.; Milbrandt, J. Sir-two-homolog 2 (Sirt2) modulates peripheral myelination through polarity protein Par-3/atypical protein kinase C (aPKC) signaling. *Proc. Natl. Acad. Sci. U. S. A.* **2011**, *108*, E952-961.
 20. (a) Pais, T. F.; Szego, E. M.; Marques, O.; Miller-Fleming, L.; Antas, P.; Guerreiro, P.; de Oliveira, R. M.; Kasapoglu, B.; Outeiro, T. F. The NAD-dependent deacetylase sirtuin 2 is a suppressor of microglial activation and brain inflammation. *EMBO J.* **2013**, *32*, 2603-2616; (b)

- 1
2
3 Zhao, T.; Alam, H. B.; Liu, B.; Bronson, R. T.; Nikolian, V. C.; Wu, E.; Chong, W.; Li, Y.
4
5 Selective inhibition of SIRT2 improves outcomes in a lethal septic model. *Curr. Mol. Med.* **2015**,
6
7 *15*, 634-641; (c) Eskandarian, H. A.; Impens, F.; Nahori, M. A.; Soubigou, G.; Coppee, J. Y.;
8
9 Cossart, P.; Hamon, M. A. A role for SIRT2-dependent histone H3K18 deacetylation in bacterial
10
11 infection. *Science* **2013**, *341*, 1238858.
12
13
14
15 21. Bae, N. S.; Swanson, M. J.; Vassilev, A.; Howard, B. H. Human histone deacetylase
16
17 SIRT2 interacts with the homeobox transcription factor HOXA10. *J. Biochem.* **2004**, *135*, 695-
18
19 700.
20
21
22 22. Jin, Y. H.; Kim, Y. J.; Kim, D. W.; Baek, K. H.; Kang, B. Y.; Yeo, C. Y.; Lee, K. Y.
23
24 Sirt2 interacts with 14-3-3 beta/gamma and down-regulates the activity of p53. *Biochem.*
25
26 *Biophys. Res. Commun.* **2008**, *368*, 690-695.
27
28
29 23. Park, S. H.; Zhu, Y.; Ozden, O.; Kim, H. S.; Jiang, H.; Deng, C. X.; Gius, D.;
30
31 Vassilopoulos, A. SIRT2 is a tumor suppressor that connects aging, acetylome, cell cycle
32
33 signaling, and carcinogenesis. *Transl. Cancer Res.* **2012**, *1*, 15-21.
34
35
36 24. Donmez, G.; Outeiro, T. F. SIRT1 and SIRT2: emerging targets in neurodegeneration.
37
38 *EMBO Mol. Med.* **2013**, *5*, 344-352.
39
40
41 25. (a) Kim, H. S.; Vassilopoulos, A.; Wang, R. H.; Lahusen, T.; Xiao, Z.; Xu, X.; Li, C.;
42
43 Veenstra, T. D.; Li, B.; Yu, H.; Ji, J.; Wang, X. W.; Park, S. H.; Cha, Y. I.; Gius, D.; Deng, C. X.
44
45 SIRT2 maintains genome integrity and suppresses tumorigenesis through regulating APC/C
46
47 activity. *Cancer Cell* **2011**, *20*, 487-499; (b) Yang, M. H.; Laurent, G.; Bause, A. S.; Spang, R.;
48
49 German, N.; Haigis, M. C.; Haigis, K. M. HDAC6 and SIRT2 regulate the acetylation state and
50
51 oncogenic activity of mutant K-RAS. *Mol. Cancer Res.* **2013**, *11*, 1072-1077.
52
53
54
55
56
57
58
59
60

- 1
2
3
4 26. (a) Luthi-Carter, R.; Taylor, D. M.; Pallos, J.; Lambert, E.; Amore, A.; Parker, A.;
5
6 Moffitt, H.; Smith, D. L.; Runne, H.; Gokce, O.; Kuhn, A.; Xiang, Z.; Maxwell, M. M.; Reeves,
7
8 S. A.; Bates, G. P.; Neri, C.; Thompson, L. M.; Marsh, J. L.; Kazantsev, A. G. SIRT2 inhibition
9
10 achieves neuroprotection by decreasing sterol biosynthesis. *Proc. Natl. Acad. Sci. U. S. A.* **2010**,
11
12 *107*, 7927-7932; (b) Chopra, V.; Quinti, L.; Kim, J.; Vollor, L.; Narayanan, K. L.; Edgerly, C.;
13
14 Cipicchio, P. M.; Lauver, M. A.; Choi, S. H.; Silverman, R. B.; Ferrante, R. J.; Hersch, S.;
15
16 Kazantsev, A. G. The sirtuin 2 inhibitor AK-7 is neuroprotective in Huntington's disease mouse
17
18 models. *Cell Rep.* **2012**, *2*, 1492-1497; (c) Bobrowska, A.; Donmez, G.; Weiss, A.; Guarente, L.;
19
20 Bates, G. SIRT2 ablation has no effect on tubulin acetylation in brain, cholesterol biosynthesis or
21
22 the progression of Huntington's disease phenotypes in vivo. *Plos One* **2012**, *7*, e34805.
23
24
25
26
27 27. (a) Cui, H.; Kamal, Z.; Ai, T.; Xu, Y.; More, S. S.; Wilson, D. J.; Chen, L. Discovery of
28
29 potent and selective sirtuin 2 (SIRT2) inhibitors using a fragment-based approach. *J. Med. Chem.*
30
31 **2014**, *57*, 8340-8357; (b) Suzuki, T.; Khan, M. N. A.; Sawada, H.; Imai, E.; Itoh, Y.; Yamatsuta,
32
33 K.; Tokuda, N.; Takeuchi, J.; Seko, T.; Nakagawa, H.; Miyata, N. Design, synthesis, and
34
35 biological activity of a novel series of human sirtuin-2-selective Inhibitors. *J. Med. Chem.* **2012**,
36
37 *55*, 5760-5773; (c) Di Fruscia, P.; Zacharioudakis, E.; Liu, C.; Moniot, S.; Laohasinnarong, S.;
38
39 Khongkow, M.; Harrison, I. F.; Koltsida, K.; Reynolds, C. R.; Schmidtkunz, K.; Jung, M.;
40
41 Chapman, K. L.; Steegborn, C.; Dexter, D. T.; Sternberg, M. J. E.; Lam, E. W. F.; Fuchter, M. J.
42
43 The discovery of a highly selective 5,6,7,8-tetrahydrobenzo[4,5]thieno[2,3-d] pyrimidin-4(3H)-
44
45 one SIRT2 inhibitor that is neuroprotective in an in vitro Parkinson's disease model.
46
47 *ChemMedChem* **2015**, *10*, 69-82; (d) Outeiro, T. F.; Kontopoulos, E.; Altmann, S. M.; Kufareva,
48
49 I.; Strathearn, K. E.; Amore, A. M.; Volk, C. B.; Maxwell, M. M.; Rochet, J. C.; McLean, P. J.;
50
51 Young, A. B.; Abagyan, R.; Feany, M. B.; Hyman, B. T.; Kazantsev, A. G. Sirtuin 2 inhibitors
52
53
54
55
56
57
58
59
60

- 1
2
3 rescue alpha-synuclein-mediated toxicity in models of Parkinson's disease. *Science* **2007**, *317*,
4 516-519; (e) Lara, E.; Mai, A.; Calvanese, V.; Altucci, L.; Lopez-Nieva, P.; Martinez-Chantar,
5 M. L.; Varela-Rey, M.; Rotili, D.; Nebbioso, A.; Ropero, S.; Montoya, G.; Oyarzabal, J.;
6 Velasco, S.; Serrano, M.; Witt, M.; Villar-Garea, A.; Imhof, A.; Mato, J. M.; Esteller, M.; Fraga,
7 M. F. Salermide, a sirtuin inhibitor with a strong cancer-specific proapoptotic effect. *Oncogene*
8 **2009**, *28*, 781-791; (f) Peck, B.; Chen, C. Y.; Ho, K. K.; Di Fruscia, P.; Myatt, S. S.; Coombes,
9 R. C.; Fuchter, M. J.; Hsiao, C. D.; Lam, E. W. SIRT inhibitors induce cell death and p53
10 acetylation through targeting both SIRT1 and SIRT2. *Mol. Cancer Ther.* **2010**, *9*, 844-855; (g)
11 Taylor, D. M.; Balabadra, U.; Xiang, Z.; Woodman, B.; Meade, S.; Amore, A.; Maxwell, M. M.;
12 Reeves, S.; Bates, G. P.; Luthi-Carter, R.; Lowden, P. A.; Kazantsev, A. G. A brain-permeable
13 small molecule reduces neuronal cholesterol by inhibiting activity of sirtuin 2 deacetylase. *ACS*
14 *Chem. Biol.* **2011**, *6*, 540-546; (h) Seifert, T.; Malo, M.; Kokkola, T.; Engen, K.; Friden-Saxin,
15 M.; Wallen, E. A.; Lahtela-Kakkonen, M.; Jarho, E. M.; Luthman, K. Chroman-4-one- and
16 chromone-based sirtuin 2 inhibitors with antiproliferative properties in cancer cells. *J. Med.*
17 *Chem.* **2014**, *57*, 9870-9888; (i) Hoffmann, G.; Breitenbucher, F.; Schuler, M.; Ehrenhofer-
18 Murray, A. E. A novel sirtuin 2 (SIRT2) inhibitor with p53-dependent pro-apoptotic activity in
19 non-small cell lung cancer. *J. Biol. Chem.* **2014**, *289*, 5208-5216.
- 20
21
22 28. Rumpf, T.; Schiedel, M.; Karaman, B.; Roessler, C.; North, B. J.; Lehotzky, A.; Olah, J.;
23 Ladwein, K. I.; Schmidtkunz, K.; Gajer, M.; Pannek, M.; Steegborn, C.; Sinclair, D. A.;
24 Gerhardt, S.; Ovadi, J.; Schutkowski, M.; Sippl, W.; Einsle, O.; Jung, M. Selective Sirt2
25 inhibition by ligand-induced rearrangement of the active site. *Nat. Commun.* **2015**, *6*, 6263.
- 26
27
28 29. (a) Schiedel, M.; Rumpf, T.; Karaman, B.; Lehotzky, A.; Olah, J.; Gerhardt, S.; Ovadi, J.;
29 Sippl, W.; Einsle, O.; Jung, M. Aminothiazoles as potent and selective Sirt2 inhibitors: A
30
31
32
33
34
35
36
37
38
39
40
41
42
43
44
45
46
47
48
49
50
51
52
53
54
55
56
57
58
59
60

- 1
2
3 structure-activity relationship study. *J. Med. Chem.* **2016**, *59*, 1599-1612; (b) Schiedel, M.;
4
5 Rumpf, T.; Karaman, B.; Lehotzky, A.; Gerhardt, S.; Ovadi, J.; Sippl, W.; Einsle, O.; Jung, M.
6
7 Structure-based development of an affinity probe for sirtuin 2. *Angew. Chem. Int. Ed.* **2016**, *55*,
8
9 2252-2256.
10
11
12
13 30. Toure, M.; Crews, C. M. Small-molecule PROTACS: New approaches to protein
14
15 degradation. *Angew. Chem. Int. Ed. Engl.* **2016**, *55*, 1966-1973.
16
17
18 31. (a) Bondeson, D. P.; Mares, A.; Smith, I. E.; Ko, E.; Campos, S.; Miah, A. H.;
19
20 Mulholland, K. E.; Routly, N.; Buckley, D. L.; Gustafson, J. L.; Zinn, N.; Grandi, P.;
21
22 Shimamura, S.; Bergamini, G.; Faelth-Savitski, M.; Bantscheff, M.; Cox, C.; Gordon, D. A.;
23
24 Willard, R. R.; Flanagan, J. J.; Casillas, L. N.; Votta, B. J.; den Besten, W.; Famm, K.;
25
26 Kruidenier, L.; Carter, P. S.; Harling, J. D.; Churcher, I.; Crews, C. M. Catalytic in vivo protein
27
28 knockdown by small-molecule PROTACs. *Nat. Chem. Biol.* **2015**, *11*, 611-617; (b) Lai, A. C.;
29
30 Toure, M.; Hellerschmied, D.; Salami, J.; Jaime-Figueroa, S.; Ko, E.; Hines, J.; Crews, C. M.
31
32 Modular PROTAC design for the degradation of oncogenic BCR-ABL. *Angew. Chem. Int. Ed.*
33
34 **2016**, *55*, 807-810.
35
36
37
38 32. (a) Sakamoto, K. M.; Kim, K. B.; Verma, R.; Ransick, A.; Stein, B.; Crews, C. M.;
39
40 Deshaies, R. J. Development of Protacs to target cancer-promoting proteins for ubiquitination
41
42 and degradation. *Mol. Cell. Proteomics* **2003**, *2*, 1350-1358; (b) Okuhira, K.; Demizu, Y.;
43
44 Hattori, T.; Ohoka, N.; Shibata, N.; Nishimaki-Mogami, T.; Okuda, H.; Kurihara, M.; Naito, M.
45
46 Development of hybrid small molecules that induce degradation of estrogen receptor-alpha and
47
48 necrotic cell death in breast cancer cells. *Cancer Sci.* **2013**, *104*, 1492-1498.
49
50
51
52 33. (a) Lu, J.; Qian, Y. M.; Altieri, M.; Dong, H. Q.; Wang, J.; Raina, K.; Hines, J.; Winkler,
53
54 J. D.; Crew, A. P.; Coleman, K.; Crews, C. M. Hijacking the E3 ubiquitin ligase cereblon to
55
56
57
58
59
60

1
2
3 efficiently target BRD4. *Chem. Biol.* **2015**, *22*, 755-763; (b) Winter, G. E.; Buckley, D. L.;
4 Paulk, J.; Roberts, J. M.; Souza, A.; Dhe-Paganon, S.; Bradner, J. E. Phthalimide conjugation as
5 a strategy for in vivo target protein degradation. *Science* **2015**, *348*, 1376-1381; (c) Zengerle, M.;
6 Chan, K. H.; Ciulli, A. Selective small molecule induced degradation of the BET bromodomain
7 protein BRD4. *ACS Chem. Biol.* **2015**, *10*, 1770-1777.

8
9
10
11
12
13
14
15 34. Lohbeck, J.; Miller, A. K. Practical synthesis of a phthalimide-based Cereblon ligand to
16 enable PROTAC development. *Bioorg. Med. Chem. Lett.* **2016**, *26*, 5260-5262.

17
18
19
20 35. Schneekloth, A. R.; Pucheault, M.; Tae, H. S.; Crews, C. M. Targeted intracellular
21 protein degradation induced by a small molecule: En route to chemical proteomics. *Bioorg. Med.*
22 *Chem. Lett.* **2008**, *18*, 5904-5908.

23
24
25
26
27 36. van Zundert, G. C.; Rodrigues, J. P.; Trellet, M.; Schmitz, C.; Kastiris, P. L.; Karaca, E.;
28 Melquiond, A. S.; van Dijk, M.; de Vries, S. J.; Bonvin, A. M. The HADDOCK2.2 web server:
29 User-friendly integrative modeling of biomolecular complexes. *J. Mol. Biol.* **2016**, *428*, 720-725.

30
31
32
33
34 37. Fischer, E. S.; Bohm, K.; Lydeard, J. R.; Yang, H.; Stadler, M. B.; Cavadini, S.; Nagel,
35 J.; Serluca, F.; Acker, V.; Lingaraju, G. M.; Tichkule, R. B.; Schebesta, M.; Forrester, W. C.;
36 Schirle, M.; Hassiepen, U.; Ottl, J.; Hild, M.; Beckwith, R. E.; Harper, J. W.; Jenkins, J. L.;
37 Thoma, N. H. Structure of the DDB1-CRBN E3 ubiquitin ligase in complex with thalidomide.
38 *Nature* **2014**, *512*, 49-53.

39
40
41
42
43
44
45 38. Kristiansen, M.; Jakobsen, P.; Lundbeck, J. M. Novel aromatic compounds. WO
46 2001023347 A1, 2001.

47
48
49
50
51 39. Cunningham, C. W.; Mukhopadhyay, A.; Lushington, G. H.; Blagg, B. S. J.; Prisinzano,
52 T. E.; Krise, J. P. Uptake, distribution and diffusivity of reactive fluorophores in cells:
53 Implications toward target identification. *Mol. Pharmaceut.* **2010**, *7*, 1301-1310.
54
55
56
57
58
59
60

- 1
2
3
4 40. (a) Huisgen, R. Centenary lecture - 1,3-dipolar cycloadditions. *P. Chem. Soc. London*
5 **1961**, 357-396; (b) Chan, T. R.; Hilgraf, R.; Sharpless, K. B.; Fokin, V. V. Polytriazoles as
6 copper(I)-stabilizing ligands in catalysis. *Org. Lett.* **2004**, *6*, 2853-2855.
7
8
9
10 41. Heltweg, B.; Trapp, J.; Jung, M. In vitro assays for the determination of histone
11 deacetylase activity. *Methods* **2005**, *36*, 332-337.
12
13
14 42. Weisberg, S. J.; Lyakhovetsky, R.; Werdiger, A. C.; Gitler, A. D.; Soen, Y.; Kaganovich,
15 D. Compartmentalization of superoxide dismutase 1 (SOD1G93A) aggregates determines their
16 toxicity. *Proc. Natl. Acad. Sci. U. S. A.* **2012**, *109*, 15811-15816.
17
18
19
20 43. Kolb, H. C.; Sharpless, K. B. The growing impact of click chemistry on drug discovery.
21 *Drug Discovery Today* **2003**, *8*, 1128-1137.
22
23
24
25 44. Neugebauer, R. C.; Uchiechowska, U.; Meier, R.; Hruby, H.; Valkov, V.; Verdin, E.;
26 Sippl, W.; Jung, M. Structure-activity studies on splitomicin derivatives as sirtuin inhibitors and
27 computational prediction of binding mode. *J. Med. Chem.* **2008**, *51*, 1203-1213.
28
29
30
31 45. Laemmli, U. K. Cleavage of structural proteins during the assembly of the head of
32 bacteriophage T4. *Nature* **1970**, *227*, 680-685.
33
34
35
36 46. Bradford, M. M. A rapid and sensitive method for the quantitation of microgram
37 quantities of protein utilizing the principle of protein-dye binding. *Anal. Biochem.* **1976**, *72*, 248-
38 254.
39
40
41
42 47. Verdonk, M. L.; Cole, J. C.; Hartshorn, M. J.; Murray, C. W.; Taylor, R. D. Improved
43 protein-ligand docking using GOLD. *Proteins* **2003**, *52*, 609-623.
44
45
46
47 48. Wang, J. M.; Wolf, R. M.; Caldwell, J. W.; Kollman, P. A.; Case, D. A. Development
48 and testing of a general amber force field. *J. Comput. Chem.* **2004**, *25*, 1157-1174.
49
50
51
52
53
54
55
56
57
58
59
60

- 1
2
3
4
5
6
7
8
9
10
11
12
13
14
15
16
17
18
19
20
21
22
23
24
25
26
27
28
29
30
31
32
33
34
35
36
37
38
39
40
41
42
43
44
45
46
47
48
49
50
51
52
53
54
55
56
57
58
59
60
49. Baell, J. B.; Holloway, G. A. New substructure filters for removal of pan assay interference compounds (PAINS) from screening libraries and for their exclusion in bioassays. *J. Med. Chem.* **2010**, *53*, 2719-2740.
50. Berthold, M. C.; Cebron, N.; Dill, F.; Gabriel, T. R.; Kötter, T.; Meinel, T.; Ohl, P.; Thiel, K.; Wiswedel, B. KNIME-the Konstanz information miner. In *Studies in Classification, Data Analysis, and Knowledge Organization*; Preisach C., Burkhardt H., Schmidt-Thieme L., Decker R., Eds.; Springer: Berlin: 2007; pp 319-326.
51. Saubern, S.; Guha, R.; Baell, J. B. KNIME Workflow to Assess PAINS Filters in SMARTS Format. Comparison of RDKit and Indigo Cheminformatics Libraries. *Mol. Inform.* **2011**, *30*, 847-850.

